Applied Catalysis B: Environmental 189 (2016) 119–132

Contents lists available at ScienceDirect

Applied Catalysis B: Environmental

journal homepage: www.elsevier.com/locate/apcatb

Catalytic supercritical gasification of biocrude from hydrothermal liquefaction of cattle manure

Mohammad S.H.K. Tushar[a], Animesh Dutta[a,*], Chunbao (Charles) Xu[b]

[a] Mechanical Engineering Program, School of Engineering, University of Guelph, Guelph, ON N1G 2W1, Canada
[b] Department of Chemical and Biochemical Engineering, Western University, London, ON N6A 5B9, Canada

ARTICLE INFO

Article history:
Received 26 October 2015
Received in revised form 30 January 2016
Accepted 12 February 2016
Available online 21 February 2016

Keywords:
Supercritical water gasification
Hydrothermal liquefaction
Biocrude
Cattle manure
Catalyst
Kinetic modelling
Eley–Rideal (ER)
Rate determining step (RDS)

ABSTRACT

In this article, we performed catalytic supercritical water gasification (SCWG) of biomass to enhance hydrogen production. First we used glucose as a model compound to screen the best catalyst and then we used this catalyst to gasify biocrude from hydrothermal liquefaction of cattle manure. We introduced a novel dual metal (Ni, Ru)—dual support (Al_2O_3, ZrO_2) catalyst for the first time in SCWG in order to improve the H_2 yield. A continuous flow tubular reactor was employed to perform the experiments. Novel 10%Ni-0.08%Ru/Al_2O_3-ZrO_2 catalyst showed the highest H_2 yield (1.34 mol/mol of C for glucose and 1.01 mol/mol of C for biocrude) and highest carbon gasiifcation efficiency (88% for glucose and 92% for biocrude). It was found that Ru promoted Ni and ZrO_2 showed some catalytic activities towards hydrogen production. The pressure was 25 MPa for all experiments. Stability test showed that 10%Ni-0.08%Ru/Al_2O_3-ZrO_2 was highly stable for a 20 h run. Among the parameters studied, higher temperature favored H_2 yield, whereas higher concentration led to lower H_2 yield. We found that carbon gasification efficiency of cattle manure biocrude was independent of variation in temperature and concentration. Also the equilibrium condition was attained at lower temperature and concentration in terms of carbon conversion of the feed. An Eley–Rideal (ER) based mechanistic model was devised and tested against the obtained data. It was found the dissociation of adsorbed oxygenated hydrocarbon is the rate determining step with an average absolute deviation 6.65%.

1. Introduction

The urge for hydrogen economy is increasing due to its cleaner combustion. Hydrogen is abundantly distributed around the world. However, it is not free and a 'suitable' technology is required to extract it from a primary source. Ninety six percent of current hydrogen demand are fulfilled from the conversion of fossil fuel [1].

The depleting nature of fossil fuel sources, strict regulations against pollution, and the unexpected price hikes necessitate the search for renewable sources for a sustainable and environmentally benign energy infrastructure. Being a local product, biomass offers environmentally friendly renewable energy resource. Increasing interest in thermochemical conversion of biomass for extracting energy has been boosted in recent years [2–4]. In contrast to the conventional thermochemical conversion process, supercritical water gasification (SCWG) of biomass does not require drying biomass, which in turn saves energy and time. The unique property of supercritical water (SCW, T_c = 373.95 °C and P_C = 22.06 MPa) allows a mass transfer limitation free reaction condition as water becomes a single phase beyond its critical point.

The heat of evaporation at higher pressure (say P > 20 MPa) becomes very insignificant comparing with ambient conditions, which means ΔH_{vap} becomes zero at P_c. Besides, hot compressed water is a promoter of ionic reactions over radical reactions, which lead to decreased char formation. In addition to this, organic molecules become more reactive in compressed water while the temperature is more than 250 °C [5,6]. These advantages stipulate a major impulse to use hot compressed water for treating various carbonaceous wastes.

SCWG using catalyst for hydrogen production is among the various processes to produce high quality fuels. Many industrial processes require hydrogen; such as the syntheses of ammonia and methanol, various hydrogenation and hydrotreating processes and most importantly, in fuel cells. Nevertheless, use of biomass as feed to produce hydrogen is gaining more attention due to the detrimental consequences on the environment by using fossil fuels. As lignocellulosic materials are the most bountiful biomass species

* Corresponding author.
E-mail address: adutta@uoguelph.ca (A. Dutta).

http://dx.doi.org/10.1016/j.apcatb.2016.02.032
0926-3373/

Nomenclature

AAD	Average absolute deviation
C_i	Concentration of various species, kmol/m^3
E	Activation energy, J/mol
k_0	Frequency factor
K_i	Adsorption constants for various species (i = 1, 2, 3. . . . .)
K_p	Equilibrium constant
n	Reaction order
N_l	Mole flow rate of various species, kmol/s
r_i	Reaction rate for a specie, kmol/kg cat s (i = A, B, C, ...)
R	Universal gas constant, kJ/kmol-K
S	Catalyst active sites
T,	Temperature, K
X_i	Conversion of component i

Subscripts

0	Reactor inlet
A	Hydrothermal oxygenated hydrocarbon
B	Water
C	Carbon dioxide
D	Hydrogen

around the world, they become eminently preferable feed material for producing biorenewable hydrogen [7]. Tentative reaction pathways of the SCWG of carbohydrates are shown in Fig. 1, adapted from Azadi et al. [8] and Cortright et al. [7]. The reactant undergoes dehydrogenation steps on the metal surface to give adsorbed intermediates before the cleavage of C—C or C—O bonds.

Due to the nutritional value and worldwide availability, cattle manure has been used as fertilizers since ancient times, as well as a fuel in developing countries. However, as the number of cattle are increasing, their excreta is being considered as waste due to methane (CH_4) emissions, which has 25 times more Global Warming Potential (GWP) compared to carbon dioxide (CO_2) on a 100-year timescale [9,10]. SCWG of liquefied cattle manure is a potential technology for the passive use of cattle manure. The major products of SCWG are hydrogen (H_2) and CO_2, and the emissions are biorganic, which means they have a negative impact on GHG emissions compared to fossil fuel.

Biomass liquefaction is one of the conversion techniques which is used to produce biocrude for further processing that can be easily transported. This biocrude contains various carbohydrates of oxygenated hydrocarbons of varying molecular structure and molecular weights, including lignin derived products, sugars and their decomposition products. In this article, an alternative approach of using cattle manure was presented. Firstly the manure was liquefied using a batch reactor at 260 °C for 30 min to produce the biocrude. This phase is aqueous, hence made it possible to pump continuously to the SCWG reactor using an HPLC pump. Secondly, this aqueous phase was then introduced into the reactor to produce an H_2 rich gas in the presence of a catalyst.

Both homogeneous (e.g., various alkali metals) and heterogeneous (e.g., transition metal catalysts, on various support) were reported by researchers to promote the water-gas shift reaction and/or C—C bond cleavage to obtain better carbon gasification efficiency and higher H_2 yield. The advantageous characteristics of the heterogeneous catalysts over homogeneous catalysts are recycleability and higher selectivity [11]. Elliott [12] and Guo et al. [11] have reported in their review about some major heterogeneous transition metal catalysts, on various supports (mainly Ni, Ru, PT, Pd, Rh etc.) that have been broadly investigated for SCWG processes. It has been reported that Ru showed the highest activity in gasifying lignin and its derivatives (alkylephenols) compared to Rh, Pd, and Pt in SCW at 400 °C [13,14]. Additionally, it was reported that Ru can maintain high stability for a longer period of time [15]. Ni is another most commonly utilized catalyst due to its ability to promote the water-gas shift reaction [16–18]. Compared to the noble metal catalysts, Ni is cheaper even though it is less stable and has the possibility of gradually losing the activity during SCWG.

Researchers used single metal single support catalysts, dual metal single support catalysts and single metal dual support catalysts to investigate SCWG of biomass [11,12]. However, dual

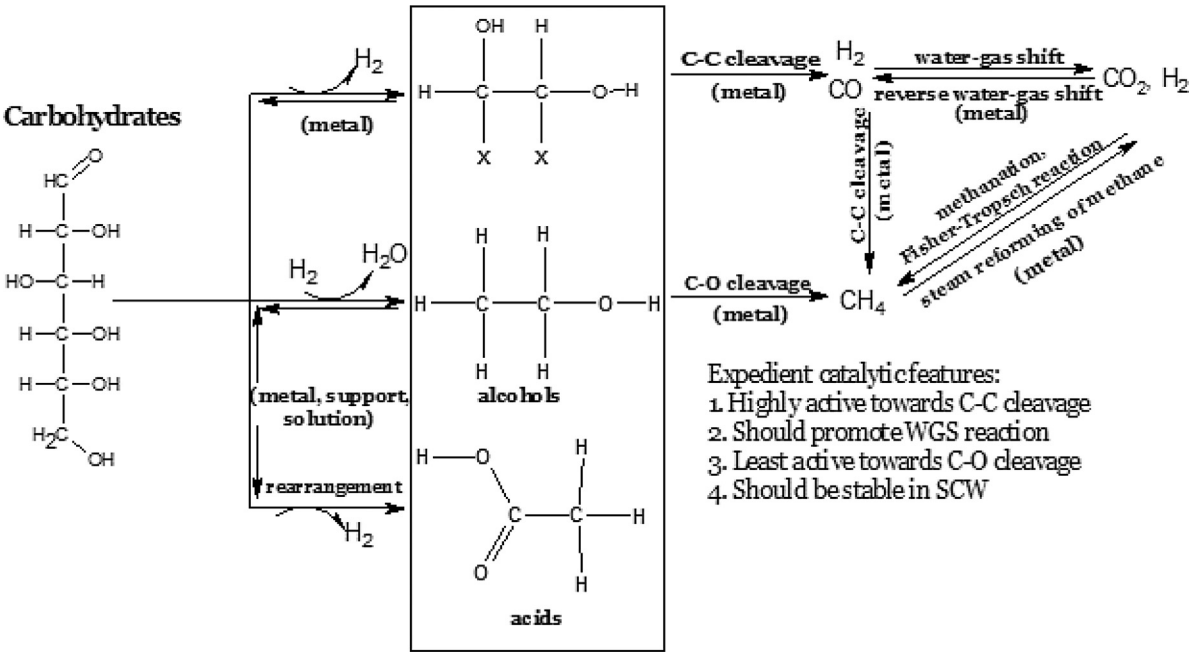

Fig. 1. Hydrogen production pathways through various reactions of oxygenated carbohydrates in the presence of water adapted from Azadi et al. [8] and Cortright et al. [7] (the □ sign represents a surface metal site).

metal dual support catalysts have yet to be investigated. As such, in this paper, we have investigated 10 different catalysts with various transition metals (Ni and Ru) and support (gamma alumina, γ-Al_2O_3 and Zirconia, ZrO_2) combinations. Gamma alumina is used in many industrial processes as catalyst support and can be taken as a benchmark to compare against [19]. Support like ZrO_2 pose some interesting properties for which they can be used as modifiers of reforming catalysts. These are improved thermal stability, increased oxygen storage ability, decrease in sintering and enhanced metallic dispersion. These properties help gasification of carbon formed during the gasification process by reforming [20,21]. For the first time, this research has investigated a dual metal dual support catalyst. Firstly a good catalyst was screened using glucose water solution, then this catalyst was used to perform SCWG of hydrothermal liquid (HTL) of cattle manure. Catalysts were characterized using BET, XRD, SEM-EDX, TEM and XPS. We devised an Eley–Rideal (ER) based mechanistic reaction scheme to obtain an intrinsic rate equation. The data was used to find the different kinetic parameters by fitting them in a basic power law model. The results of these derivations, the findings of the experiments and the analyses are discussed in this research.

2. Materials and methods

2.1. Feedstock and catalyst preparation

Cattle manure was collected from the University of Guelph livestock farm. HTL of cattle manure was carried out using a Parr Instrument 600 ml bench top batch reactor (Moline, IL) equipped with a glass liner (762HC3) shown elsewhere [22]. Experiments were performed at 260 °C for 30mins with a feedstock-to-water ratios 1:6 (w/w). 10 g of 'as received' cattle manure samples were mixed with 60 g of deionized water and was stirred for about 3 min. The HTL procedure is also described elsewhere [22]. For the screening experiments, 50 g of α-D-glucose (dextrose monohydrate, MP Biomedicals, LLC) was dissolved in 1 L deionized water to reach the concentration of 50 g/L. The incipient wetness impregnation method was used to prepare catalysts with single metal and co-impregnation method was used to prepare binary catalysts [18]. Nickel (II) nitrate hexahydrate, $Ni(NO_3)_2{\cdot}6H_2O$ and ruthenium (III) nitrosyl nitrate solution in dilute nitric acid, $HN_4O_{10}Ru$ are used as metal precursors and obtained from Sigma-Adlrich. For alumina supported catalysts, spherical γ-Al_2O_3 (dia. = 1.8 mm) were used which are supplied by Sasol. The support materials for dual support catalysts are γ-Al_2O_3 and ZrO_2 supplied by Fisher Scientific. Catalysts were calcined at 600° C for 5 h and then stored in an air-tight bag. Prior to the experiment, the catalysts were ground and sieved (using ASTM standard sieve sizes 20 and 50, Fisher Scientific) to average catalyst diameter of 575 μm.

2.2. Apparatus and experimental procedure

Fig. 2 shows the schematic diagram of the SCWG reactor used in this experiment. A 12.84 mm OD × 9.28 mm ID × 660.67 mm length tubular reactor with continuous feed flow, fabricated from Inconel 625 was used to perform the experiments. Reactor tube was packed with previously crushed and sieved catalyst, which are supported on a stainless steel membrane (mesh 80). A small amount (2 cm in depth) of quartz wool was placed in between the catalyst support rod and the screen to avoid the possible carry-away of catalyst particles. An electrical heater was used to heat the packed reactor to the desired temperature. Once the reactor reached the reaction temperature, the in-situ reduction of the catalyst was performed by supplying hydrogen at a rate of 5 ml/min for 90 min. Hydrogen gas was then used through the high-pressure line to pre-pressurize the reactor. The liquid feedstock was then introduced into the system by using a HPLC (high pressure low capacity) pump from Eldex (optos series) at 5 mL/min. Once the system reached the desired reaction pressure, the feed flow is reduced to the experimental flow rate 2 mL/min which translates to weight hourly space velocity (WHSV) of 2 h^{-1}. Once the system is stabilized, the first gas sample was taken after one hour. Gas sampling was done once per hour for a duration of 10 min for each sampling time. The liquid produced during this time was also being collected, weighed and stored for further analysis. During all the experiments, pressure remained constant at 25 MPa. Three different temperatures (500, 600 and 700 °C), and carbon concentrations (10, 15 and 20 g/L) were studied for the hydrothermal liquid. Prior to using catalysts, a suitable temperature was chosen based on higher hydrogen production by running experiments without catalysts. Then the best catalyst was chosen by running the experiments using the prepared ten catalysts. All of these experiments were performed using glucose. Then the best catalyst was used to perform gasification experiment using the hydrothermal liquid produced from cattle manure at different conditions.

Table 1
Ultimate and Proximate analysis.

Proximate Analysis of Cattle Manure (CM), wt%	
Vloatile matter (DAF)	80.02
Moisture content	65.40
Ash content (D)	1.49
Fixed carbon	18.49
Ultimate Analysis of Cattle Manure, wt%	
Nitrogen	1.39
Carbon	45.02
Hydrogen	6.10
Sulphur	0.16
Oxygen	47.33
Ultimate Analysis of dried biocrude from CM, wt%	
Nitrogen	2.04
Carbon	39.48
Hydrogen	5.14
Sulphur	0.14
Oxygen	53.20

2.3. Characterization

2.3.1. Cattle manure characterization

The proximate analysis was performed according to the ASTM standards using a Thermo Scientific- F48055-60, Waltham, and MA muffle furnace. For moisture content, ash content, and volatile matter, ASTM-E871, ASTM-E1755, and ASTM- E872 were used, respectively. Fixed carbon is then calculated by using (100%-volatile matter- ash content). A Thermo Fisher Flash EA 1112, Waltham, MA elemental analyser was used to perform elemental analysis of the biomass samples. Table 1 shows the proximate and ultimate analysis of cattle manure and ultimate analysis of HTL.

2.3.2. HTL biocrude characterization

The chemical composition of biocrudes from the HTL process were analyzed using an Agilent VF-5 ms phenyl–methyl GC column (30 m × 0.25 mm id with a film thickness 0.25-μm) with a Bruker Daltonics Scion TQ GC–MS/MS (Bruker Daltonics, Fremont, CA) system. Helium was the carrier gas with a flow rate of 1 mL/min. 1 μL of dichloromethane (DCM) extracts (contains 2 wt% biocrude) were injected at oven temperature of 270 °C using a split ratio of 30:1. The initial oven temperature was set to 60 °C and was held for 4 min, then raised to 280 °C with the heating rate of 5 °C/min and held for 15 min. The data was collected over the mass to charge ratio

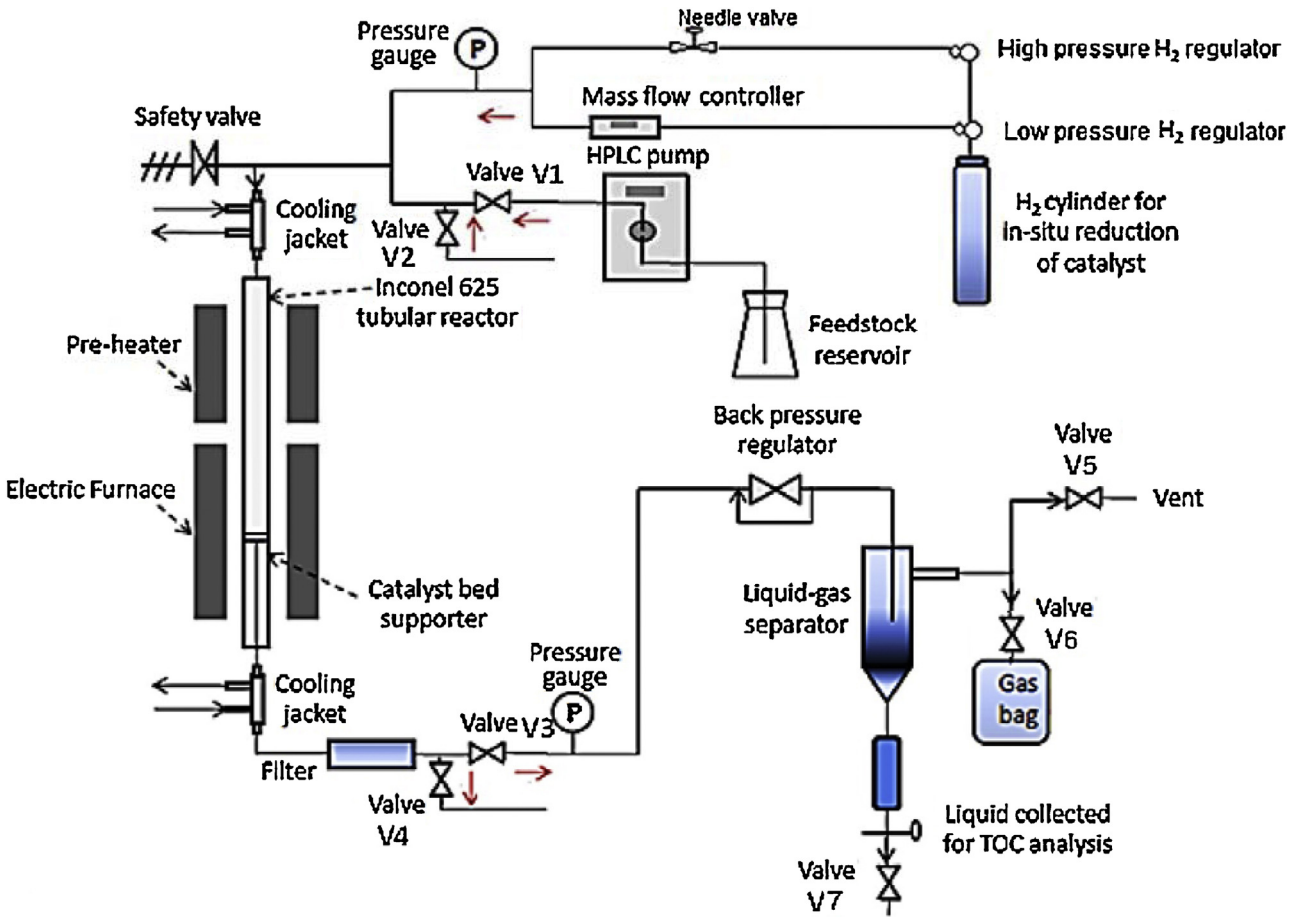

Fig. 2. Schematic diagram of the experimental setup.

(*m*/*z*) range from 35 to 550 with a source temperature of 210 °C and electron ionization of 70 eV. The time per scan was 0.2 s with an interscan delay of 0.1 s. Individual compound identification was performed by matching the peak patterns against a NIST database. Matlab was used to correct the baseline and to filter the signal noise prior to the peak integration.

2.4. Catalysts characterization

Brunauer–Emmett–Teller (BET) Analysis was performed using a Quantachrome 4200e Surface Area and Pore Analyser. First the samples were placed in the sample holder and degassed in vacuum for three hours at room temperature. The weight of the samples were recorded before and after degassing to address any mass loss. Samples were then placed for BET analysis in the analyser. Prior to each run, the tubes were calibrated using helium gas. N_2 physisorption was then performed at liquid nitrogen temperature. The isotherm was recorded over the pressures range from $0.03 < P/Po < 0.4$. Table 2 shows the summary of catalysts BET surface area.

X-ray diffraction (XRD) patterns for powdered on the dried and calcined catalysts samples were performed using a STOE goniometer and Cu Kα radiation (λ = 1.5406 Å) at room temperature. The background noise level was minimized by using an energy sensitive 2500 Silicon drift detector from Moxtek. The 2θ scanning was performed with a rate of 5°/min and a range of 20–65° while the voltage and current were 35 kV and 40 mA respectively.

The spent catalysts from 6 h-run and 20 h-run were analysed in order to investigate the char produced using an SDT Q600 thermogravimetric analyser (TGA), DSC-TGA Standard from TA Instrument. A heating rate of 20 °C/min was used to heat the spent catalyst samples placed in an alumina crucible to the final temperature 900 °C using an air flow of 40 mL/min.

FEI Inspect S50 scanning electron microscope (SEM) equipped with a tungsten filament and an Everhart-Thornley secondary electron (SE) detector was used with a working distance of approximately 10 cm, a spot size of 3.5, and a 30 kV electron beam energy for all SEM images. The energy dispersive spectroscopy (EDS) spectra were collected with an Oxford X-max 20 with Aztec Software using a spot size of 3.5 with an accelerating voltage of 30 kV to ensure that the Ru K(alpha) line at 19.24 keV was excited.

Transmission electron microscopy of the catalyst particles was performed using a Tecnai G2 F20 (FEI, Hilsboro, OR) equipped with a 4K Gatan GT digital camera (Gatan, Pleasanton, CA). A 300-mesh carbon grid was used to mount the samples. Digital Microgram software was used for controlling the image quality.

A PE5600 XPS system (Physical Electronics, Chanhassen, MN), equipped with a monochromatic A1 Kα X-ray source (operates at 350 W), multichannel detector and hemispherical analyser, was used to perform X-Ray photoelectron spectroscopy (XPS). Catalyst samples were mounted on an indium foil. Charge was neutralised using a low-energy electron flood gun (~1 eV). Two different spectra were collected using different energy and step sizes. Analyser pass energy and step size for survey spectra were 187.85 eV and 0.8 eV per step respectively and for high resolution spectra were 23.50 eV and 0.1 eV per step respectively. CasaXPS software (http://www.casaxps.com) was used to analyse the data.

Table 2
Catalyst compositions and physical characteristics.

Sl no.	Catalysts	Metal content (wt.%)	Support	BET surface area (m^2/g)	Total pore volume (cc/g)	Average pore radius (Å)
1	–	–	γ-Al_2O_3 (P[a])	0.669	0.002	15.423
2	–	–	γ-Al_2O_3 (S[a])	170.666	0.395	46.797
3	–	–	ZrO_2	8.691	0.015	27.982
4	5%Ni/Al_2O_3	5%Ni	γ-Al_2O_3	143.685	0.249	43.724
5	10%Ni/Al_2O_3	10%Ni	γ-Al_2O_3	132.552	0.227	43.488
6	0.04%Ru/Al_2O_3	0.04%Ru	γ-Al_2O_3	83.924	0.132	18.063
7	0.08%Ru/Al_2O_3	0.08%Ru	γ-Al_2O_3	169.048	0.47	46.895
8	5%Ni-0.04%Ru/Al_2O_3	5%Ni + 0.04%Ru	γ-Al_2O_3	173.289	0.425	60.056
9	10%Ni-0.08%Ru/Al_2O_3	10%Ni + 0.08%Ru	γ-Al_2O_3	160.471	0.383	43.756
10	5%Ni-0.04%Ru/ZrO_2	5%Ni + 0.04%Ru	ZrO_2	6.191	0.017	16.945
11	10%Ni-0.08%Ru/ZrO_2	10%Ni + 0.08%Ru	ZrO_2	6.446	0.025	18.131
12	5%Ni-0.04%Ru/Al_2O_3-ZrO_2	5%Ni + 0.04%Ru	γ-Al_2O_3+ ZrO_2	3.382	0.013	15.353
13	10%Ni-0.08%Ru/Al_2O_3-ZrO_2	10%Ni + 0.08%Ru	γ-Al_2O_3+ ZrO_2	5.178	0.021	22.961

[a] P = Powder, S = Sphere.

2.5. Gas characterization

Gas analysis was carried out using an 8610C GC (SRI Instruments, Torrance, CA) which has two columns (molecular sieve; Porapak). It is equipped with two detectors: a thermal conductivity detector (TCD) and a flame ionization detector (FID). A standard gas mixture (Linde) was used for the calibration of this GC. Helium is used the carrier gas.

2.6. Theory

2.6.1. Kinetic modeling

In this study, an effort is made with elementary steps of SCWG in the presence of catalysts. Accordingly mechanistic models applying Eley–Rideal (ER) mechanism is proposed and will be verified using the experimental data. The slowest step, also termed as rate determining step (RDS) will be determined. The overall SCWG reaction of HTL of cattle manure is given below.

$$C_{10}H_{16}O_{10} + 10H_2O \rightarrow 10CO_2 + 18H_2;\ \Delta H^{\circ}298 = 107.6\text{kJ/mol} \quad (1)$$

At first, an empirical and irreversible rate model based on power law (PL) for HTL conversion in SCW with a fixed feed concentration, r_A (concentration/time) is developed as shown below:

$$r_A = k_r C_A^n = k_0 e^{-\frac{E}{RT}} C_A^n \quad (2)$$

$$\text{Where, } k_r = k_0 e^{-\frac{E}{RT}} \quad (3)$$

k_0 = pre-exponential factor (frequency factor)
n = reaction order
E = activation energy, J/mol
C_A = concentration of cattle manure (CM) dry oil in kmol/m^3.

The unknown k_0, E and n are approximated using NLREG®, a multi-linear regression software, of the experimental data. Nevertheless, reaction rate constant, k_r has variable units as it is related to reaction order.

Secondly, mechanistic models based on ER are developed. According to the model, a catalyst active site interacts only with dissolved carbohydrate. The steps are as follows:

$$C_{10}H_{16}O_{10} + [S] \overset{k_{1,-1}}{\leftrightarrow} C_{10}H_{16}O_{10}[S] \quad \text{(absorption)} \quad (4)$$

$$C_{10}H_{16}O_{10}[S] + [S] \overset{k_{2,-2}}{\leftrightarrow} \underset{\text{Benzenehexol}}{C_6H_6O_6[S]} + \underset{\text{Erythrytol}}{C_4H_{10}O_4[S]} \quad (SR-I) \quad (5)$$

$$\underset{\text{Benzenehexol}}{C_6H_6O_6[S]} + 6H_2O + 5[S] \overset{k_{3,-3}}{\leftrightarrow} 9H_2 + 6CO_2[S] \quad (SR-II) \quad (6)$$

Table 3
Various rate models formulated ER mechanisms.

Model No.	Equation	Eq. No.
ER1	$r_A = \frac{k_0 e^{-\frac{E}{RT}}\left(C_A - \frac{C_C^{10} C_D^{18}}{K_P C_B^{10}}\right)}{\left(1 + K_A C_A + \frac{K_B C_C^6 C_D^9}{C_B^6} + K_C C_C + \frac{K_D C_C^4 C_D^9}{C_B^4}\right)^2}$	(9)
ER2	$r_A = \frac{k_0 e^{-\frac{E}{RT}}\left(\frac{C_A C_B^{10}}{C_C^4 C_D^9} - \frac{C_C^6 C_D^9}{K_P}\right)}{\left(1 + K_A C_A + \frac{K_B C_A C_B^4}{C_C^4 C_D^9} + K_C C_C + \frac{K_D C_C^4 C_D^9}{C_B^4}\right)^6}$	(10)
ER3	$r_A = \frac{k_0 e^{-\frac{E}{RT}}\left(\frac{C_A C_B^6}{C_C^6 C_D^9} - \frac{C_C^4 C_D^9}{K_P}\right)}{\left(1 + K_A C_A + \frac{K_B C_C^6 C_D^9}{C_B^4} + K_C C_C + \frac{K_D C_A C_B^4}{C_C^6 C_D^9}\right)^4}$	(11)

$$\underset{\text{Erythrytol}}{C_4H_{10}O_4[S]} + 4H_2O + 3[S] \overset{k_{4,-4}}{\leftrightarrow} 9H_2 + 6CO_2[S] \quad (SR-III) \quad (7)$$

$$10CO_2[S] \overset{k_{5,-5}}{\leftrightarrow} 10CO_2 + 10[S] \quad \text{(Desorption)} \quad (8)$$

SR = surface reaction, [S] = Active sites on catalysts, k_i = rate of forward reaction, k_{-i} = rate of backward reaction

It is well known that a chemical reaction consists of more than one step, termed as elementary steps, and there is one step which is the slowest compared to the others. This slowest elementary step is the decider for the overall reaction rate and hence it is called a rate determining step (RDS). Owing to the unique property to remain unchanged during chemical reactions, catalysts are not shown in the equation. Nevertheless, their presence can clearly be seen in the proposed rate equations as shown by active sites. Eqs. (4) and (8) were not used to develop any model. In total, three ER models were devised and investigated. Table 3 shows all the models and related assumptions on these reactions.

3. Results and discussion

3.1. Non-catalytic supercritical water gasification

Since the primary goal of this study is to enhance the hydrogen yield, several non-catalytic experiments were performed to find the suitable condition of higher hydrogen production. The pressure was 25 MPa with the temperatures 500, 600 and 700 °C and a feed (5 wt% glucose-water solution) flow of WHSV of 2 h^{-1}. Fig. 3 shows comparison of gas yield and carbon gasification efficiency (CGE) at various temperature. It is clearly seen from the Figure that higher temperature favored hydrogen and carbon dioxide yield

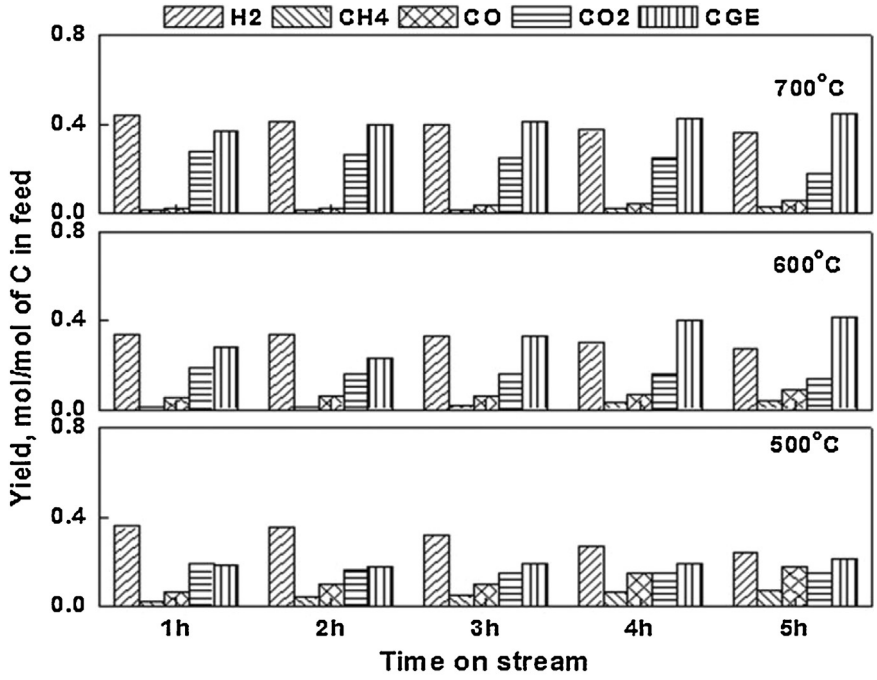

Fig. 3. Gas yields from SCWG of 5 wt.% glucose-water solution without any catalyst, P = 25 MPa.

(Eq. (12)). However, with the increase in time, both hydrogen and carbon dioxide production decreased.

$$CO + H_2O \leftrightarrow CO_2 + H_2 \quad (12)$$

$$CH_4 + 2H_2O \leftrightarrow CO_2 + 4H_2 \quad (13)$$

As hydrogen production is endothermic and methane production exothermic, with the increase in temperature an increase in hydrogen yield and decrease in methane yield observed as stated in Le Chatelier's principle. However, with the increase in time, carbon deposition on the inner wall of the reactor led to less heat transfer which in turn caused diminishing trends of hydrogen and carbon dioxide and increasing trends of methane and carbon monoxide (reverse water gas shift, Eq. (12) and methanation reaction, Eq. (13)) [23]. Based on the results obtained in non-catalytic SCWG for higher hydrogen yield, for catalytic gasification, T = 700 °C was chosen.

3.2. Effect of different metal catalysts

It is very important to pick the catalysts as it should not only able to gasify the feedstock but also able to gasify the intermediates and byproducts which usually lead to tar production. Fig. 4 shows hydrogen yield and CGE using ten catalysts with different metal loadings (Ni, Ru) on various supports (γ-Al_2O_3 and ZrO_2) in SCW at 700 °C and 25 MPa for 5 h time on-stream.

There are two points to consider: (1) Data used for plotting graphs and analyses were averaged which were acquired at steady state. This is done when the gas yields with various composition becomes almost constant with time-on-stream. (2) The reactor is fabricated from Inconel which mainly consists of Ni (58%), Cr (20–23%), Mo (8–10%), Fe (Max 5%), Nb (3.15–4.15%) and with some trace elements. Thusly, the reactor could involve in catalysing SCWG process. Besides this reactor could be termed as "seasoned" or "aged" due to slow and steady catalytic effect [24]. According to Kruse [24], this reactor could be considered as a "seasoned" or "aged" reactor with low and constant catalytic effect. Since all of the experiments (with and without catalysts) were conducted using the same reactor, the effects of reactor wall on gas yield were considered to be comparable for all experimental conditions and thus will not be discussed in this work.

Compared to Fig. 3, it can be found that both hydrogen production and CGE increased in the presence of catalysts. Among the catalysts used for gasification, 5%Ni/Al_2O_3 showed the poorest catalyst activity and 10%Ni-0.08%Ru/Al_2O_3-ZrO_2 showed the best catalyst activity in terms of hydrogen yield and carbon gasification efficiency. Nickel is known for its catalytic activity on water-gas shift reaction [25]. Addition of small amount of Ru also aid in hydrogen production [26]. As per Figs. 3 and 4, hydrogen yield increases from on average 32% (5%Ni/Al_2O_3) to 200% (10%Ni-0.08%Ru/Al_2O_3-ZrO_2). Compared to 10%Ni-0.08%Ru/Al_2O_3, 10%Ni-0.08%Ru/Al_2O_3-ZrO_2 showed better hydrogen yield even though it has lower surface area. As it is mentioned in the Introduction part, ZrO_2 aid in gasification process by reforming, it played the important role to higher hydrogen yield and higher CGE which can be clearly seen from Fig. 4. Fig. 5 shows that using ZrO_2 as support has increased CO_2 yield and decreased both CH_4 and CO yield which also justifies the statement. As 10%Ni-0.08%Ru/Al_2O_3-ZrO_2 exhibited higher hydrogen yield compared to other catalysts, it is further used for gasifying the hydrothermally liquefied (HTL) cattle manure. Besides, this catalyst further characterized for better understanding.

3.3. Stability tests on 10%Ni-0.08%Ru/Al_2O_3-ZrO_2

According to the outcomes discussed above, 10%Ni-0.08%Ru/Al_2O_3-ZrO_2 was termed as the best catalyst. Hence, it is important to explore the stability of it by running experiments for extended period of time using the same experimental conditions. The 20 h long run was split in three days. On first day the experiment ran for 8 h, then the experiment ran for 6 h on second and third day. During this longer running experiment, neither plugging nor deactivation was detected. Gas yield and carbon gasification efficiency (CGE) of 5 wt% glucose water solution at 700 °C at 25 MPa in the presence of 10%Ni-0.08%Ru/Al_2O_3-ZrO_2 for time on stream 20 h are shown in Fig. 6. It is evident from the Figure that the catalyst prevailed its high activity during whole running

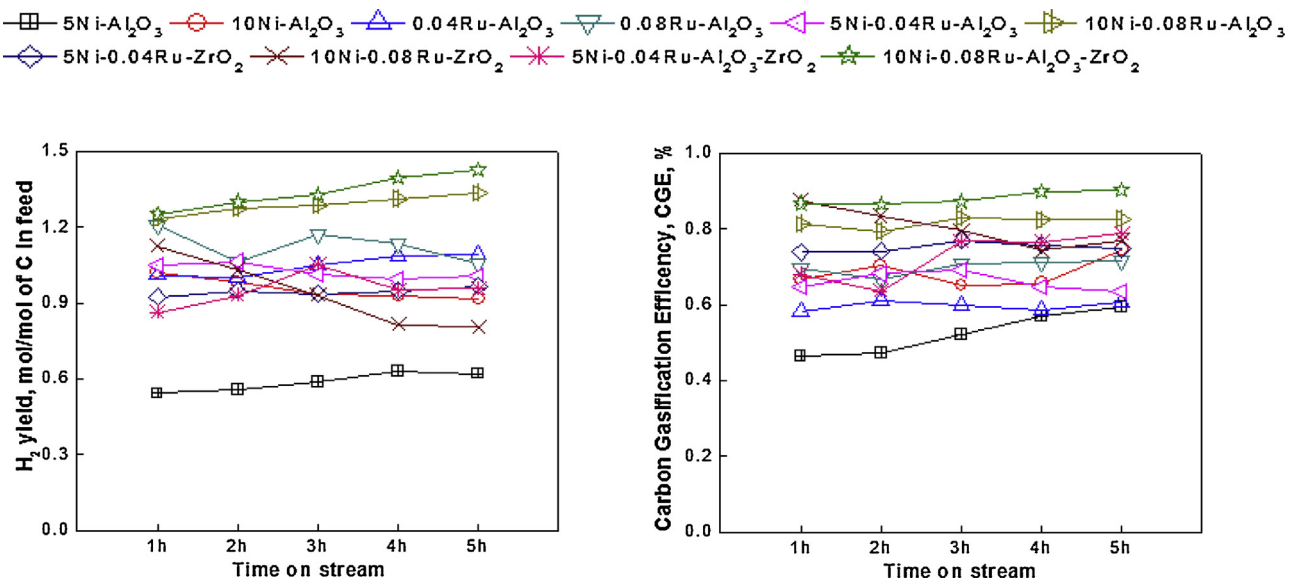

Fig. 4. Hydrogen yield and carbon gasification efficiency from SCWG of 5 wt.% glucose-water solution at 700 °C and 25 MPa in the presence of catalysts.

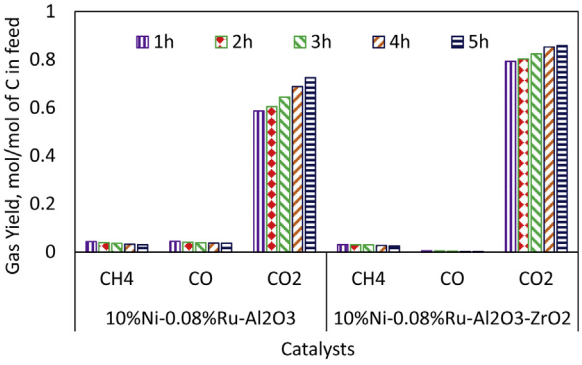

Fig. 5. CH_4, CO_2 and CO yield of SCWG of 5 wt.% glucose-water solution at 700 °C and 25 MPa.

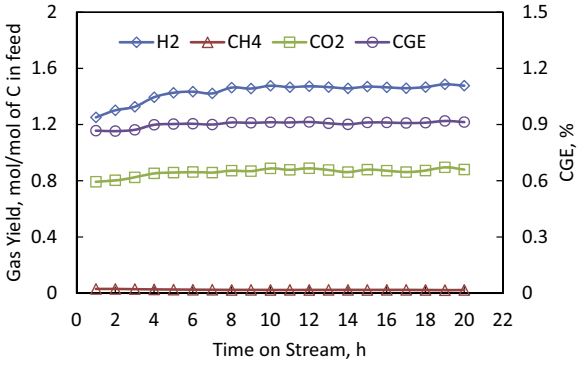

Fig. 6. Gas yield and CGE at 5 wt.% glucose-water solution 700 °C and 25 MPa for a 20 h run.

period. Plugging is the widely experienced problem in continuous flow reactor due to tar and char deposition and agglomeration on catalysts. Besides, sintering (due to high temperature) of the particles, support material decomposition and catalyst metal leaching are other frequent issues of using heterogeneous catalysts in continuous flow reactor. To investigate these problems, fresh and used 10%Ni-0.08%Ru/Al_2O_3-ZrO_2 were characterized using SEM-EDX, XRD and TGA.

Fig. 7 shows SEM-EDX analysis of both fresh (not reduced) and used 10%Ni-0.08%Ru/Al_2O_3-ZrO_2. The magnification for the fresh catalyst was 250 μm and for the used catalyst was 100 μm. Although it is not possible explain the dispersion of catalyst metal particles in the supports due to limitations in resolution of SEM, the EDX spectra shows the different elements presents in the specimen. The spectra shows Ni, Ru, Al, Zr, and O elements and the used catalyst also shows C, which means some carbon deposited on the catalyst surface. This confirms char and/or coke generation and deposition on the catalyst surface. The slivers seen in used catalyst SEM image are indication of char and/or coke.

Fig. 8 shows the TEM images of fresh and spent 10%Ni-0.08%Ru/Al_2O_3-ZrO_2 catalyst. The fresh catalyst particles have slightly rough surfaces. Rough surface of catalyst particles are indication of poor crystallinity. These surfaces cause the formation of random graphene layers which eventually lead to the formation of Turbostatic (T-) carbon [27] which could not be separated from the amorphous carbon using TEM [26]. Zhang et al. [26] also found the same carbon structure in their research. The arrow showed the area where the T-carbon formed on the used catalyst (b). These findings are further investigated using the TGA.

Fig. 9 illustrates the XRD patterns for not reduced fresh and in-situ reduced spent 10%Ni-0.08%Ru/Al_2O_3-ZrO_2 catalyst. Since the amount of Ru was too low, the XRD was not able to identify the either RuO or Ru. The instrument is capable of identifying any element if it is present at least 0.1 wt% in the mixture. As per the illustration, fresh catalyst contains the oxides of supports and nickel. The XRD pattern of fresh and not-reduced catalyst shows three peaks of NiO at 37.2°, 43.4° and 63.4° [28–32]. However, the metallic form of Ni was identified in the used catalyst at 44.6 and 51.8° [30,32]. This is due to the in-situ reduction performed before the experiment and in-reaction reduction occurred by H_2 and CH_4 which are known as reducing gases. Ni peaks observed by XRD are the active sites of the spent catalyst for SCWG [26]. Besides, a peak of α- Al_2O_3 is observed at 43.3 which conforms the phase transformation of Al_2O_3 from γ to α [26]. In conclusion after careful observation of the XRD patterns, the metal Ni remain in metallic form after the 5 h run using glucose at 700 °C and 25 MPa. It can also be assumed from the conclusions of previous studies, Ru also remains in metallic form after each experiment [28]. Thus, these active metallic Ni and Ru are responsible for consistent higher activity of 10%Ni-0.08%Ru/Al_2O_3-ZrO_2 catalyst.

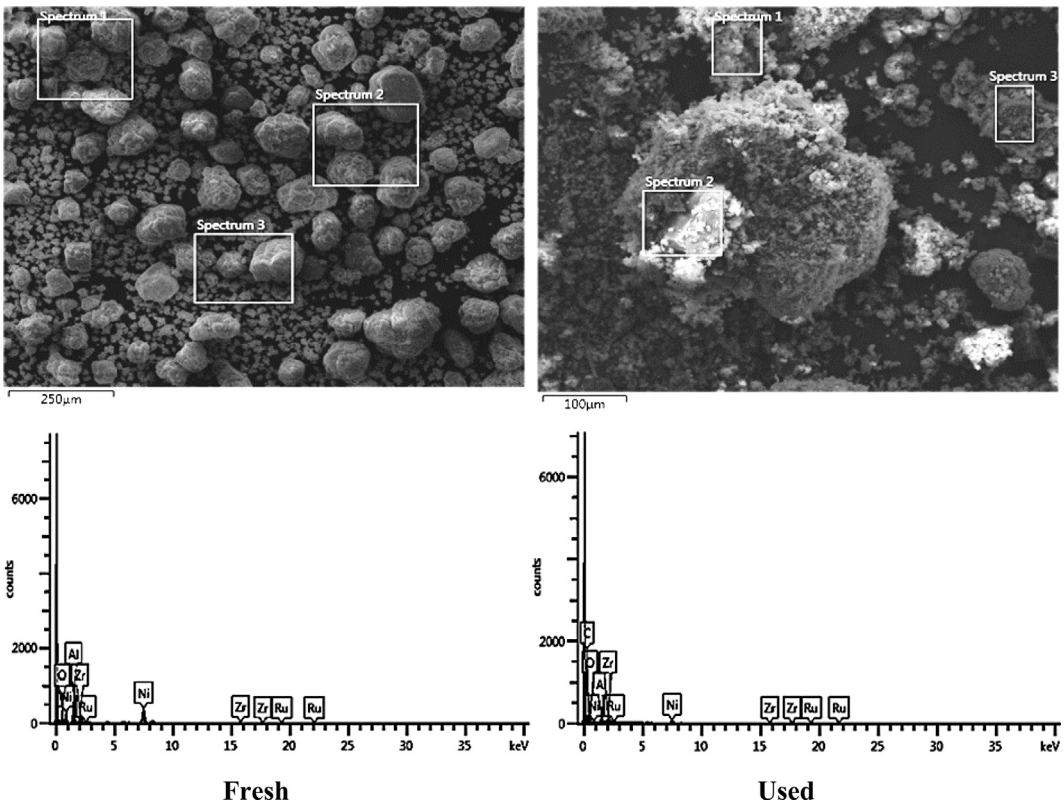

Fig. 7. SEM images and EDX spectra for the fresh (not reduced) and used 10%Ni-0.08%Ru/Al_2O_3-ZrO_2 catalyst.

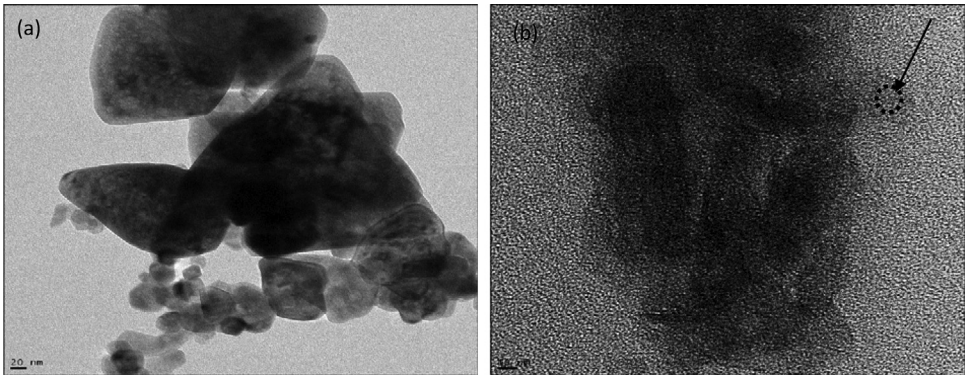

Fig. 8. TEM images for the fresh (a, not reduced) and used (b) 10%Ni-0.08%Ru/Al_2O_3-ZrO_2 catalyst. The bar scales are 20 nm for (a) and 10 nm for (b).

Fig. 10 illustrates the XPS spectra of both fresh and used catalysts 10%Ni-O. 08% Ru/Al_2O_3–ZrO_2. The XPS spectra are shown for fresh catalyst in (a-Ni), (c-Ru, C), (e-O), (g-Zr) and (i-Al) and for spent catalyst in (b-Ni), (d-Ru, C), (f-O), (h-Zr) and (j-Al). In order to determine the oxidation state, the binding energies (BE) and chemical shifts of Ni and Ni-oxides in the XPS spectra can be used [33]. As per Table 4, the Ni2p spectra showed just over 1 eV increase in BE in case of spent catalyst which is a proof of atomic sputtering [34]. Since Ru was not identified through XRD, XPS analyses were performed in order to support the presence of Ru in the catalyst. As it can be seen from the Figure, Ru was clearly detected by XPS. In Fig. 10(c) of the fresh catalyst, stepped peaks are detected in 280.85 and 284.85 eV. The first peak attributed to ruthenium 3d and the later peak is assigned as carbon 1s [35]. Also Ru3p peak is detected at 460.05 eV [36].

Fig. 11 shows the TGA profiles of the spent 10%Ni-0.08%Ru/Al_2O_3-ZrO_2 catalysts at different time on stream conditions. The char produced are mainly consists of two different types of carbon [37,38]: amorphous form of carbon and graphite-like structure, which prove the two stage mass loss of catalyst chars. Usually moisture evaporation and combustion of amorphous carbons are accountable for the mass loss under 300 °C, whereas coke combustion, mainly graphitic carbon, is responsible for the mass loss at higher temperature [39]. It is demonstrated by Zhang et al.

Table 4
Binding Energy Values of the 10%Ni-0.08% Ru/Al_2O_3–ZrO_2 Catalyst for XPS Spectra.

Name	Binding energy, eV	
	fresh catalyst	used catalyst
Al 2p	68.05	68.05
C 1s	284.85	284.59
Ni 2p	851.35	852.75
O 1s	526.55	528.65
Ru 3p	460.05	460.05
Zr 3d	177.95	178.65

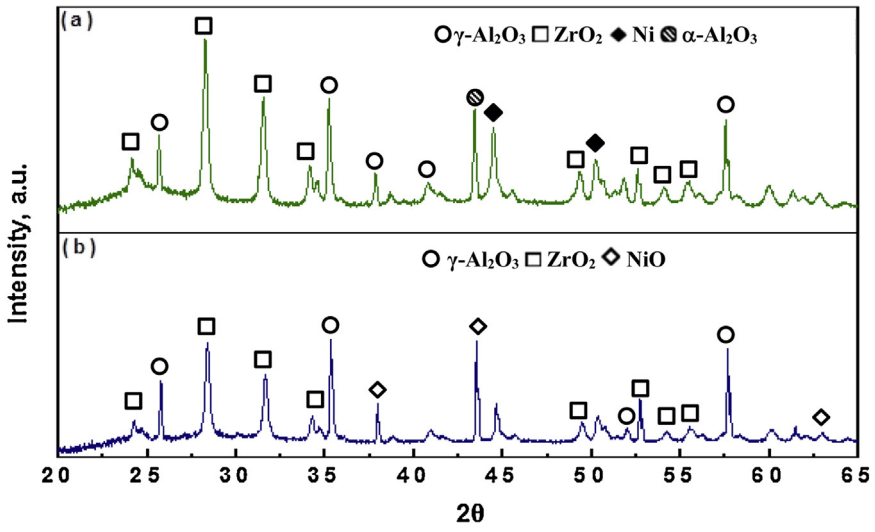

Fig. 9. XRD patterns for used (a) after 5 h time on stream and fresh (b) 10%Ni-0.08%Ru/Al_2O_3-ZrO_2.

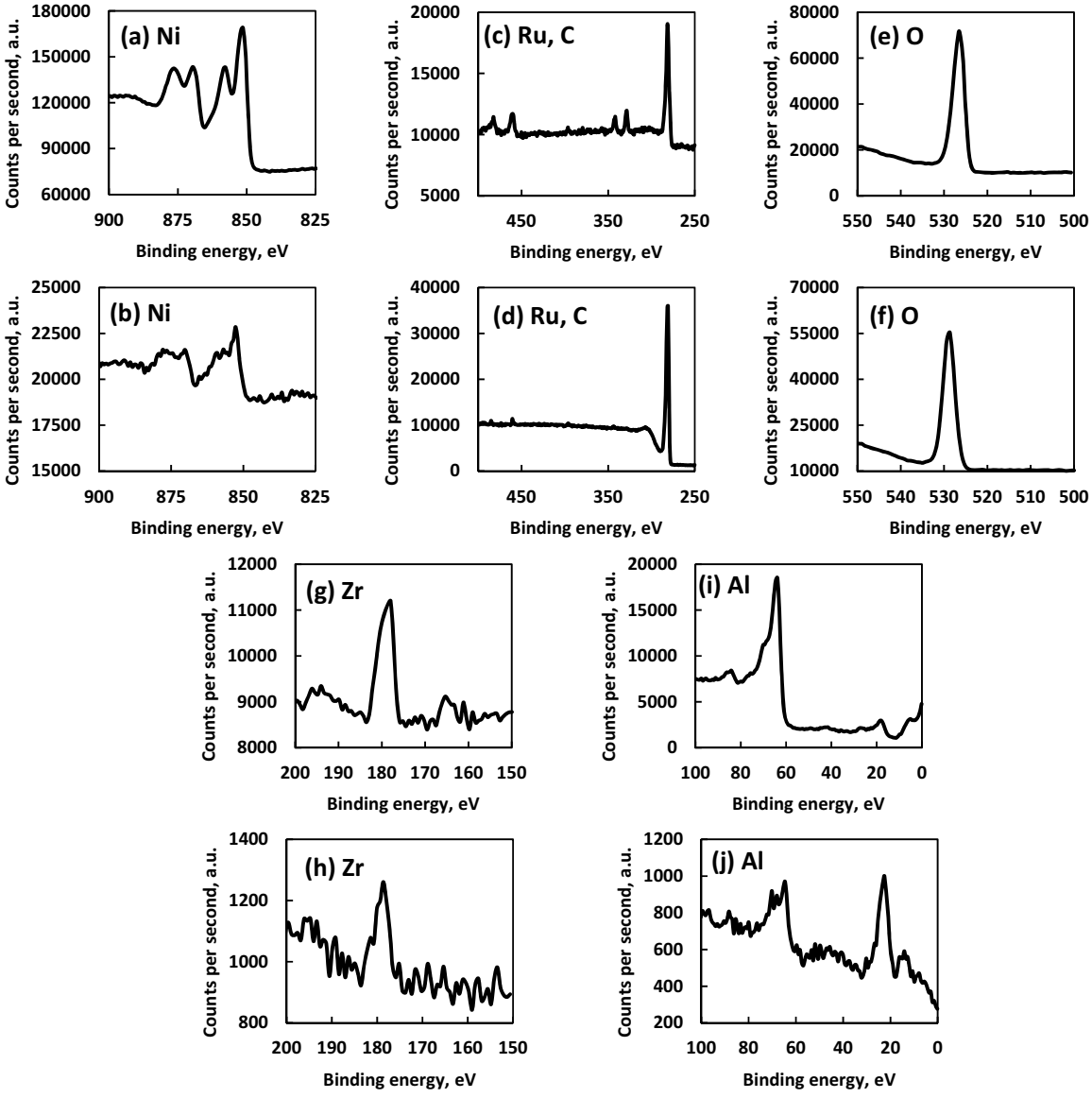

Fig. 10. XPS spectra of fresh ((a), (c), (e), (g), (i)) and spent ((b), (d), (f), (h), (j)) 10%Ni-0.08%Ru/Al_2O_3-ZrO_2 catalyst.

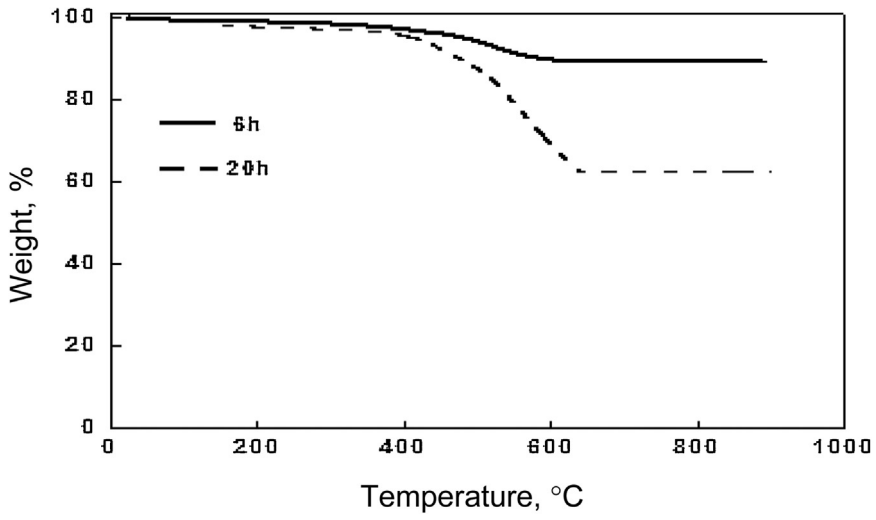

Fig. 11. TGA profiles for 10%Ni-0.08%Ru/Al_2O_3-ZrO_2 after 6 h and 20 h run.

[26] that Ni catalyst promoted by Ru produced comparatively less char/tar. Also char/tar formation and deposition is usually minimized due to the presence of ZrO_2 [40]. As per Fig. 11, the novel dual metal-dual support catalyst has accumulated carbon amount about 11% after 6 h and about 36% after 20 h' time on stream. Nevertheless, the char formed due to the accumulation of carbon on catalyst did not seem to deactivate our novel catalyst. This result corroborate with the findings of SEM and TEM in terms of char formation.

3.4. Biocrude composition

Biocrude produced by hydrothermal liquefaction was characterized by GC–MS. Due to the unstable nature of biocrude, it was observed that some black carbonaceous substances were precipitated [41]. Hence, the biocrude was filtered twice using vacuum suction filtration with a 2.5 μm filter paper prior to the experiment. Table 5 shows tentative biocrude composition. As the biocrude has very complex composition, it is not possible to attain perfect separation of the component peaks. It is a well-known fact that biocrude from biomass through hydrothermal liquefaction contain a vast range of organic compounds with complex composition [42,43]. Overall, the major components were phenolic compounds, ketones, esters, aldehydes, carboxylic acids, and furan.

Table 5
Tentative GC–MS characterization of biocrude of cattle manure representing >1% total ion chromatogram areas.

Compound	Area, %
Phenol, 2-methoxy-	9.72
Phenol, 4-ethyl-2-methoxy-	5.41
2,4-Dimethoxyphenol	7.73
Ethanone, 1-(4-hydroxy-3,5-dimethoxyphen	7.28
Total phenolic compounds	30.14
2(3H)-Benzofuranone, 3a,4,5,7a-tetrahydr	2.37
Glutaraldehyde	
Spirohexan-5-one	
1,3-Cyclopentanedione, 2-methyl-	
5-Octen-1-ol, (Z)-	
Octahydrochromen-2-one	
1,2-Cyclopentanediol, *trans*-	
Acetic acid, nonyl ester	
Cyclononanone	
1-Nonanol	
2-Cyclohexen-1-one, 4-(1-methylethyl)-	
9-Dodecen-1-ol, acetate, (Z)-	
Benzaldehyde, 3-hydroxy-4-methoxy-	
Tetracyclo[5.3.1.1(2,6). 0(4,9)]dodecan-3-one	
2-Propenoic acid, tridecyl ester	
7-Ethyl-4,6-pentadecandione	
Oxiraneoctanoic acid, 3-octyl-, *cis*-	
Pentanedioic acid, dibutyl ester	
Hexadecane, 1-methoxy-13-methyl-	
Pentadecanoic acid, 3-methylbutyl ester	
1,2-Cyclohexanedicarboxylic acid, di(3-methylbut-2-yl) ester	

3.5. Effects of temperature on SCWG of biocrude

HTL biocrude with carbon content 10 g/L was investigated in the presence of 10%Ni-0.08%Ru/Al_2O_3-ZrO_2 at temperatures from 500 to 700 °C at pressure 25 MPa with a feed flow of 2 mL/min. The results are summarized in Fig. 13.With the increase in temperature, hydrogen and carbon dioxide yield decreases and methane yield increases. Besides, the carbon gasification efficiency also decreases with the increase in temperature. This is due to the presence of phenolic and furan compounds, which gradually deactivate the catalyst. It is reported by Kruse et al. [44] that the presence of phenols or phenolic compounds along with furfurals and furan form tar and char will eventually deactivate the catalyst. According to the GC–MS characterization, the biocrude contains 30.14% of phenolic compounds and 2.37% furan compound. Even though, there were no evidence of furfurals in biocrude; nevertheless, any furfural generated during HTL process of cattle manure may transform into furans as the HTL temperature was 260 °C. Hoydonckx et al. [45] reported that furfurals start to decompose to furans beyond the temperature 250 °C. As such, deactivation of the catalyst may also be due to the furan content even though the amount is very small (2.37%). H_2 and CO_2 yields increase and CH_4 yield decreases when the reaction temperature increases. According to the thermodynamics, CH_4 and water is formed from H_2 and CO_2 at lower reaction temperatures through the methanation reaction. Contrary to this, the methanation reaction is inhibited at higher temperature by promoting the water gas shift reaction, which leads to low methane and carbon monoxide formation. Besides, the excess water present in a SCWG boosts the yield of H_2 and CO_2 rather than CO.

3.6. Effects of feed concentration on SCWG

Feed concentration is another important parameter that directly affects the gas generation. Usually lower feed concentration yield H_2 rich gas and vice versa [46,47]. High water content of the feed serves as not only solvent but also an important reactant, which

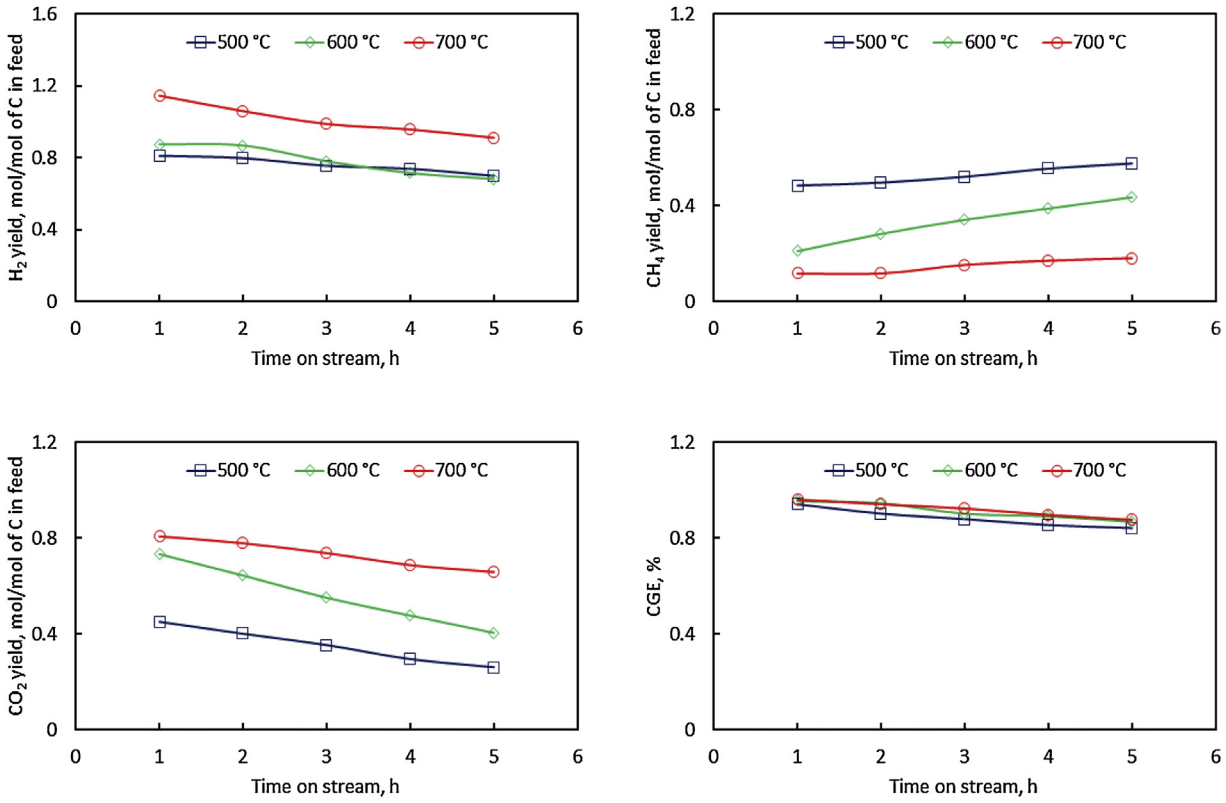

Fig. 12. Effect of temperature on gas yield and CGE; P = 25 MPa, feed flow = WHSV of 2 h^{-1}, 10 g/L C cattle manure biocrude, catalyst = 10%Ni-0.08%Ru/Al_2O_3- ZrO_2.

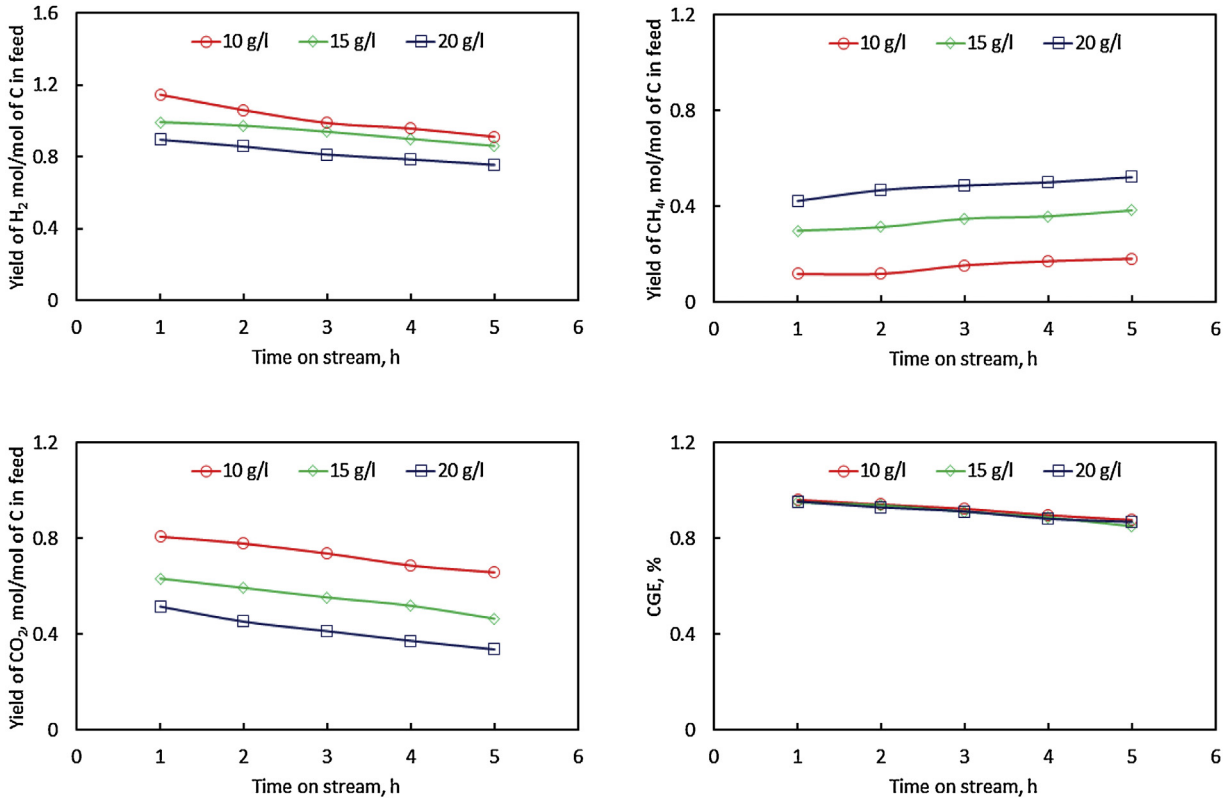

Fig. 13. Effect of concentration on gas yield and CGE; P = 25 MPa, feed flow = WHSV of 2 h^{-1}, cattle manure biocrude, catalyst = 10%Ni-0.08%Ru/Al_2O_3- ZrO_2.

Table 6
Comparison of hydrogen yield and CGE to other researches.

Study and experimental conditions	Catalytic condition	Hydrogen Yield (mol/mol$_{carbon}$)	Carbon Gasification Efficiency
Present study Cattle manure biocrude (700 °C, 25 MPa)	No catalyst	0.50	0.89
	Ni10%-Ru0.08%/Al_2O_3-ZrO_2	1.10	0.95
Zhang et al. Sludge and waste newspaper biocrude (700 °C, 24 MPa)	No catalyst	0.52	0.90
	Ni10%-Ru0.1%/Al_2O_3	0.49	0.97
	Ni10%-Ru0.1%/AC	0.85	0.92
Byrd et al. Switchgrass biocrude (600 °C, 25 MPa)	Ru/TiO_2	0.81	0.78
	Ru/ZrO_2	–	0.67
	Ni/TiO_2	0.69	0.74
	Ni/ZrO_2	0.95	0.96
	Co/TiO_2	0.56	0.83
	Co/ZrO_2	0.71	1.02

directly takes part in the process [13]. Efficient advancement of solvation reaction takes place when the biomass to water ratio is comparatively lower during heat-up thusly lowering the possibility of producing the precursors of coke/tar/char, the polymerized carbonaceous materials. At high feed concentration, the polymerization reactions are stimulated by the formation of obstinate species as intermediates from the feed, thusly reducing the available molecules for gasification. Higher feed concentration leads to higher CH_4 yield due to less amount of water available for the process, which restricts the steam reforming of methane [48]. Fig. 13 shows the effect of concentration on gas yield and CGE. The feed concentration used in this case are 10, 15 and 20 g/L of carbon (C). A feed containing 5 g/L C did not yield any sufficient amount of gas and feed containing C content higher than 20 g/L lead to blockage of the feed transfer line. According to the Figures, the result greatly corroborates with the literature articles discussed above.

3.7. Other catalytic biocrude SCWG attributes

As mentioned earlier, this study has introduced the novel concept of dual metal-dual support catalyst applied for the first time in case of the SCWG process. After careful observation of the effects of temperature and concentration on product yield, it can be easily seen that, the production of hydrogen and CO_2 was slowly decreased with an increase in methane and CO with the increase in time and feed concentration. Also lower temperature favoured methane production through methanation reaction (reverse methane reforming equation, Eq. (13)). The presence of phenolic and furan compounds led to catalyst deactivation in terms of hydrogen production for longer running period. However, it can be easily observed from Figs. 12 and 13, CGE slowly decreased with the increase in reaction time and thusly can be said that CGE is almost independent of temperature and concentration. Besides, it can also be said that, the equilibrium condition can be attained at lower temperature and concentration in terms of carbon conversion of the feed.

Table 7
Estimate of the values of the parameters of the models.

Parameters	PL	ER1	ER2
k0	3.47×10^6	1.87×10^7	2.00×10^{39}
E, J/mol	7254.89	6500	27783.10
n	1.06	–	–
K_A	–	1.00×10^9	1.00×10^{14}
K_B	–	1	1
K_C	–	6.07×10^5	1
K_D	–	1	1

3.8. Comparison with previous study

A comparison with previous studies for the first 2.5 h run are shown in Table 6. Byrd et al. [29] and Zhang et al. [49] performed continuous flow SCWG using liquefied biomass with almost similar parameters. The corresponding parent feedstock and experimental parameters are also mentioned in the table. According to the comparison, the Ni10%-Ru0.08%/Al_2O_3-ZrO_2 catalyst showed highest H_2 yield and fourth highest CGE. The catalyst activity for H_2 yield can be shown Ni10%-Ru0.08%/Al_2O_3-ZrO_2 > Ni/ZrO_2 > Ni10%-Ru0.1%/AC > Ru/TiO_2 whereas for the CGE by the catalysts

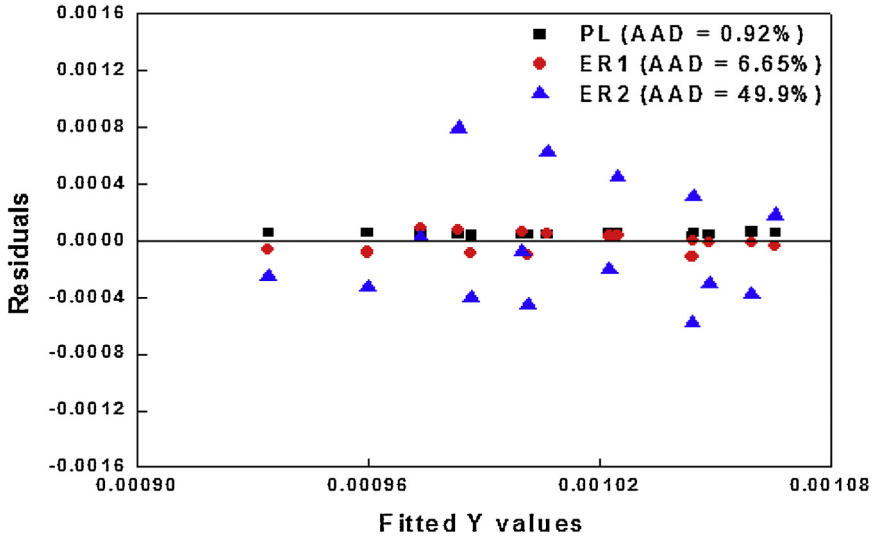

Fig. 14. Residual plot of the fitted values.

can be shown as Co/ZrO_2 > Ni10%-Ru0.1%/Al_2O_3 > Ni/ZrO_2 > Ni10%-Ru0.08%/Al_2O_3-ZrO_2. Zhang et al. [49] has reported that Al_2O_3-supported Ni catalyst lost its activity very fast whereas the catalyst supported on AC showed comparatively higher activity and stability while the real biomass derived biocrude was used. Byrd et al. [29] also mentioned that ZrO_2 supported catalysts showed higher biocrude conversion but faced plugging after a few hours due to excessive char formation. They also mentioned TiO_2 supported catalysts showed the lowest char formation although the hydrogen yield was comparatively lower. In the present study, the highest hydrogen yield and CGE was observed using Ni10%-Ru0.08%/Al_2O_3-ZrO_2 without any reactor plugging, which means addition of small amount of Ru and using ZrO_2 can significantly improve H_2 yield comparable to higher Ru catalysts. As Ru is costly, this research showed that addition of smaller amount in the catalyst will be very cost effective. Nevertheless, H_2 yield decreased slowly over time as catalyst lost its activity due to the presence of phenolic compounds and furans in HTL.

3.9. Estimation of the rate model parameters and validation

NLREG®, a nonlinear regression software, was used to estimate the model parameters. Table 7 shows the various parameters obtained through regression for converged models and the power law (PL) model. For the validation of models, AAD (average absolute deviation) in percentage was calculated and compared between the experimental and predicted reaction rates. Comparing the convergence of the models, only two models were converged. Further investigation were performed by considering AAD ≤15% and by comparing the activation energies of converged models to that of the PL model. After careful observation of the restrictions, only one model showed acceptability to predict the SCWG of the HTL of cattle manure.

Fig. 14 shows the residual plot for PL and converged ER models. As per the plot, it can be concluded that the power law model (Eq. (2), AAD ≤5%) and ER1 (Reaction 5, rate Eq. (8), AAd ≤ 10%) converged with satisfactory results and thusly the dots tightly adhere to the zero baseline. However, ER2 did converge with high AAD (=49%) for which the dots are more scattered around the zero baseline. Besides the AAD, model ER1 also showed comparable activation energy with that of PL model. By considering the values from data, the thermodynamic equilibrium constant and by using the model parameter values, model ER1 can be rearranged as follows:

$$r_A = \frac{1.87 \times 10^7 e^{-\frac{6500}{8.314T}} C_A}{\left(1 + 1.00 \times 10^9 C_A + 6.07 \times 10^5 C_C\right)^2} \quad (14)$$

The reduced Eq. (14) was basically derived from rate Eq. (9). Based on the discussion above, it can be said that model ER1 can be the RDS. In other words, dissociation of the carbohydrate needs two active sites, which make this step slower; thusly making it the RDS. So the hydrocarbon dissociation requires a longer time frame before going to the next step of the reaction.

4. Conclusion

In this study, we investigated dual metal dual support catalyst for the first time in order to enhance hydrogen yield. Nickel and ruthenium metal catalysts were supported on γ-Al_2O_3 and ZrO_2. Higher temperature favoured higher hydrogen yield, whereas higher concentration led to higher methane yield. Compared to non-catalytic gasification, use of a catalyst showed better gas yield. Among the catalysts tested, 10%Ni-0.08%Ru/Al_2O_3-ZrO_2 showed the highest hydrogen production and carbon gasification efficiency for both glucose (1.24 mol/mol of carbon and 90.29% respectively) and for HTL biocrude from cattle manure (1.01 mol/mol of carbon and 92.00% respectively). The results also showed that water directly takes part in the reaction, which attribute to higher H_2 yield. The support ZrO_2 exhibited some catalytic activity. The same catalyst showed better stability in terms of hydrogen production and carbon gasification efficiency. The HTL contains a higher amount of phenolic compounds. Hence, the catalyst becomes poisoned while running HTL as a feedstock, as indicated by the decreasing trend of H_2 yield. As expected, higher feed concentration led to comparatively more carbon deposition; however, no tar was observed using HTL as a feedstock. It was observed that carbon gasification efficiency of cattle manure biocrude was independent of variation in temperature and concentration. At lower temperature and concentration, the equilibrium condition was attained in terms of carbon conversion of the feed. By comparing with other researches, it is also found that Ni10%-Ru0.08%/Al_2O_3-ZrO_2 showed higher hydrogen yield. An ER based mechanistic model and dissociation of carbohydrate, found to be the RDS with AAD 6.65%. In terms of activation energy, this ER model showed great agreement with the empirical and simple power law rate model, $r_A = 3.47 \times 10^{06} e^{-\frac{7.25\times10^3}{RT}} C_A^{1.05}$ with an AAD of 0.93%. In future, the catalyst will be tested against different feedstock to check its universal applicability.

Acknowledgements

We acknowledge the funding from NSERC via the Discovery Grant Program (400495). We also acknowledge the XRD analyses by Dr. Lawrence Margulies, Post-Doctoral Fellow, Department of Physics; the BET analyses by Dr. Jay Leitch, Nanoscience Laboratory Technician; TEM analysis by Robert (Bob) Harris, manager, Microscopy Imaging Facility and the GC–MS analyses by Dr. Dyanne Brewer, Manager, Mass Spectrometry Facility, Associate Graduate Faculty, Advanced Analysis Centre, University of Guelph, ON. We gratefully acknowledge the XPS analyses by Dr. Mark C. Biesinger, Manager, Research and Business Development, Surface Science Western, Western University.

References

[1] B. Acharya, A. Dutta, P. Basu, Energy Fuel 23 (10) (2009) 5077–5083.
[2] N.L. Panwar, R. Kothari, V.V. Tyagi, Renew. Sust. Energy Rev. 16 (4) (2012) 1801–1816.
[3] S. Nanda, J. Mohammad, S.N. Reddy, J.A. Kozinski, A.K. Dalai, Biomass Convers. Biorefin. 4 (2) (2014) 157–191.
[4] E. Kirtay, Energy Convers. Manag. 52 (4) (2011) 1778–1789.
[5] W. Bühler, E. Dinjus, H.J. Ederer, A. Kruse, C. Mas, J. Supercrit. Fluids 22 (1) (2002) 37–53.
[6] J.M.L. Penninger, R.J.A. Kersten, H.C.L. Baur, J. Supercrit. Fluids 16 (2) (1999) 119–132.
[7] R.D. Cortright, R.R. Davda, J.A. Dumesic, Nature 418 (6901) (2002) 964–967.
[8] P. Azadi, E. Afif, F. Azadi, R. Farnood, Green Chem. 14 (6) (2012) 1766–1777.
[9] C.H. Burton, C. Turner, Silsoe Research Institute Bedford, UK, 2003.
[10] P. Forster, V. Ramaswamy, P. Artaxo, T. Berntsen, R. Betts, D.W. Fahey, J. Haywood, J. Lean, D.C. Lowe, G. Myhre, J. Nganga, R. Prinn, G.M.S. Raga, R. Van Dorland, Climate Change 2007: The Physical Science Basis. Contribution of Working Group I to the Fourth Assessment Report of the Intergovernmental Panel on Climate Change, in: S. Solomon, D. Qin, M. Manning, Z. Chen, M. Marquis, K.B. Averyt, M. Tignor, H.L. Miller (Eds.), Cambridge University Press, Cambridge, UK and New York, NY, USA, 2007, pp. 129–234.
[11] Y. Guo, S.Z. Wang, D.H. Xu, Y.M. Gong, H.H. Ma, X.Y. Tang, Renew. Sust. Energy Rev. 14 (2010) 334–343.
[12] D.C. Elliott, Biofuels Bioprod. Biorefin. 2 (3) (2008) 254–265.
[13] A. Yamaguchi, N. Hiyoshi, O. Sato, K.K. Bando, M. Osada, M. Shirai, Catal. Today 146 (1) (2009) 192–195.
[14] T. Sato, M. Osada, M. Watanabe, M. Shirai, K. Arai, Ind. Eng. Chem. Res. 42 (19) (2003) 4277–4282.
[15] F.L. Resende, P.E. Savage, Ind. Eng. Chem. Res. 49 (6) (2010) 2694–2700.
[16] M. Inaba, K. Murata, M. Saito, I. Takahara, Energy Fuel 20 (2) (2006) 432–438.
[17] T. Furusawa, T. Sato, H. Sugito, Y. Miura, Y. Ishiyama, M. Sato, et al., Int. J. Hydrogen Energy 32 (6) (2007) 699–704.
[18] I.G. Lee, S.K. Ihm, Ind. Eng. Chem. Res. 48 (3) (2008) 1435–1442.
[19] H. Pines, W.O. Haag, J. Am. Chem. Soc. 82 (10) (1960) 2471–2483.

[20] T.G. Kuznetsova, V.A. Sadykov, S.A. Veniaminov, G.M. Alikina, E.M. Moroz, V.A. Rogov, O.N. Martyanov, V.F. Yudanov, I.S. Abornev, S. Neophytides, Catal. Today 91–92 (2004) 161–164.
[21] F. Dong, A. Suda, T. Tanabe, Y. Nagai, H. Sobukawa, H. Shinjoh, M. Sugiura, C. Descorme, D. Duprez, Catal. Today 90 (1–2) (2004) 223–229.
[22] H.S. Kambo, A. Dutta, Appl. Energy 135 (2014) 182–191.
[23] Y. Calzavara, C. Joussot-Dubien, G. Boissonnet, S. Sarrade, Energy Convers. Manag. 46 (4) (2005) 615–631.
[24] A. Kruse, Biofuels. Bioprod. Biorefin. 2 (2008) 415–437.
[25] C. Ratnasamy, J.P. Wagner, Catal. Rev. Sci. Eng. 51 (3) (2009) 325–440.
[26] L. Zhang, P. Champagne, C.C. Xu, Int. J. Hydrogen Energy 36 (16) (2011) 9591–9601.
[27] W.H. Lin, T.T. Lee, Y.Y. Li, J. Taiwan Inst. Chem. Eng. 45 (4) (2014) 1883–1891.
[28] I. Behnia, MESc Diss, The University of Western Ontario, London, 2013, pp. 53.
[29] A.J. Byrd, S. Kumar, L. Kong, H. Ramsurn, R.B. Gupta, Int. J. Hydrogen Energy 36 (5) (2011) 3426–3433.
[30] C. Wang, N. Sun, M. Kang, X. Wen, N. Zhao, F. Xiao, W. Wei, T. Zhao, Y. Sun, Catal. Sci. Technol. 3 (9) (2013) 2435–2443.
[31] M. Rezaei, S.M. Alavi, S. Sahebdelfar, P. Bai, X. Liu, Z. Yan, Appl. Catal. B-Environ. 77 (3) (2008) 346–354.
[32] Y. Matsumura, T. Nakamori, Appl. Catal. A-Gen. 258 (1) (2004) 107–114.
[33] A.P. Grosvenor, M.C. Biesinger, R.S.C. Smart, N.S. McIntyre, Surf. Sci. 600 (9) (2006) 1771–1779.
[34] R. Razzaq, H. Zhu, L. Jiang, U. Muhammad, C. Li, S. Zhang, Ind. Eng. Chem. Res. 52 (6) (2013) 2247–2256.
[35] J. Du, X.X. Yang, J. Ding, X.L. Wei, J.P. Yang, W.L. Wang, M.L. Yang, J. Cent. South Univ. 20 (2013) 1307–1313.
[36] Z.B. Wang, P.J. Zuo, G.P. Yin, J. Alloys Compd. 479 (1) (2009) 395–400.
[37] M.S.H.K. Tushar, N. Mahinpey, A. Khan, H. Ibrahim, P. Kumar, R. Idem, Biomass Bioenergy 37 (2012) 97–105.
[38] S. Wang, G.Q.M. Lu, J. Chem. Technol. Biotechnol. 75 (7) (2000) 589–595.
[39] K.Y. Koo, H.S. Roh, Y.T. Seo, D.J. Seo, W.L. Yoon, S.B. Park, Appl. Catal. A-Gen. 340 (2) (2008) 183–190.
[40] F. Pompeo, N.N. Nichio, M.M.V.M. Souza, D.V. Cesar, O.A. Ferretti, M. Schmal, Appl. Catal. A-Gen. 316 (2) (2007) 175–183.
[41] A. Chuntanapum, Y. Matsumura, Ind. Eng. Chem. Res. 48 (22) (2009) 9837–9846.
[42] D.R. Vardon, B.K. Sharma, J. Scott, G. Yu, Z. Wang, L. Schideman, et al., Bioresour. Technol. 102 (17) (2011) 8295–8303.
[43] C.S. Theegala, J.S. Midgett, Bioresour. Technol. 107 (2012) 456–463.
[44] A. Kruse, T. Henningsen, A. Sinag, J. Pfeiffer, Ind. Eng. Chem. Res. 42 (16) (2003) 3711–3717.
[45] H.E. Hoydonckx, W.M. Van Rhijn, D.E. De Vos, P.A. Jacobs, Ullmann's Encycl. Ind. Chem. (2007).
[46] L.J. Guo, Y.J. Lu, X.M. Zhang, C.M. Ji, Y. Guan, A.X. Pei, Catal. Today 129 (3) (2007) 275–286.
[47] Y. Lu, L. Guo, X. Zhang, C. Ji, Int. J. Hydrogen Energy 37 (4) (2012) 3177–3185.
[48] X.H. Hao, L.J. Guo, X. Mao, X.M. Zhang, X.J. Chen, Int. J. Hydrogen Energy 28 (1) (2003) 55–64.
[49] L. Zhang, P. Champagne, C. Xu, Bioresour. Technol. 102 (17) (2011) 8279–8287.